Nanoscale

PAPER

View Article Online
View Journal | View Issue

Cite this: *Nanoscale*, 2023, **15**, 3796

Bubble-blowing-inspired sub-micron thick freestanding silk films for programmable electronics†

Qingsong Li, *[a] Fengjiao Bai,[b] Jing Sun,[a] Xiaomeng Zhou,[a] Wei Yuan, [c] Jin Lin,[a] Ke-Qin Zhang, *[b] Guanglin Li[a] and Zhiyuan Liu *[a]

Thin film electronics that are capable of deforming and interfacing with nonplanar surfaces have attracted widespread interest in wearable motion detection or physiological signal recording due to their light weight, low stiffness, and high conformality. However, it is still a challenge to fabricate freestanding thin film substrates or matrices with only sub-micron thickness in a simple way, especially for those materials with metastable conformations, like regenerated silk protein. Herein, we developed a dip-coating method for the fabrication of sub-micron thick freestanding silk films inspired by blowing soap bubbles. Using a closed-loop frame to dip-coat in a concentrated silk fibroin aqueous solution, the substrate-free silk films with a thickness as low as hundreds of nanometres (~150 nm) can be easily obtained after solvent evaporation. The silk films have extremely smooth surfaces (R_q < 3 nm) and can be tailored with different geometric shapes. The naturally dried silk films possess random coil dominated uncrystallized secondary structures, exhibiting high modulation ability and adaptability, which can be conformally attached on wrinkled skin or wrapped on human hair. Considering the methodological advantages and the unique properties of the obtained sub-micron thick silk films, several thin film based programmable electronics including transient/durable circuits, skin electrodes, transferred skin light-emitting devices and injectable electronics are successfully demonstrated after being deposited with gold or conducting polymer layers. This research provides a new avenue for preparing freestanding thin polymer films, showing great promise for developing thin film electronics in wearable and biomedical applications.

Received 3rd October 2022,
Accepted 2nd January 2023

DOI: 10.1039/d2nr05490f

rsc.li/nanoscale

Introduction

Soft and stretchable electronics have attracted significant interest worldwide due to their facile applications in wearable motion detection, healthcare monitoring, human–machine interactions, and implantation.[1–3] Generally, most of the electronic devices using plastic or elastic films (like polyethylene terephthalate, polyurethane, polyimide, silicone, *etc.*)[4] are micron to millimetre thick, and cannot build a reliable device–tissue interface for high-quality signal recording or intuitive interaction. It has been reported that when the film thickness is decreased to several microns or nanometres, conformal contact with improved interface performance can be achieved.[5,6] These ultrathin films are lightweight and exhibit lower stiffness, higher conformality, and better wearability compared with conventional rigid and thick films,[7] having been used as important building blocks of high-performance and deformable microelectronics including transistors, electronic tattoos, and skin electrodes.[8–13] Although several strategies like spin-coating,[11] dip-coating,[14] physical/chemical vapor deposition,[15,16] interfacial assembly,[17,18] electrospinning,[19] and their combinations[20,21] have been utilized to prepare thin films with low thickness and have truly improved device performance, they need to be either released from the rigid substrates *via* additionally dissolving sacrificial layers or handled/transferred in liquids, which is not only time consuming but also may affect the shapes and properties of the films. More importantly, with the demand for better biocompatibility and functionality of electronic devices (like biosensors, transient and programmable devices) in recent years, various biomaterials (like silk protein) and programmable materials are emerging.[22–24] These novel materials are usually metastable

[a]*CAS Key Laboratory of Human-Machine Intelligence-Synergy Systems, Shenzhen Institute of Advanced Technology, Chinese Academy of Sciences (CAS), Shenzhen 518055, China. E-mail: qs.li@siat.ac.cn, zy.liu1@siat.ac.cn*
[b]*National Engineering Laboratory for Modern Silk, College of Textile and Clothing Engineering, Soochow University, Suzhou 215123, China. E-mail: kqzhang@suda.edu.cn*
[c]*Printable Electronics Research Centre, Suzhou Institute of Nano-Tech and Nano-Bionics, Chinese Academy of Sciences, Suzhou, 215123, China*
† Electronic supplementary information (ESI) available. See DOI: https://doi.org/10.1039/d2nr05490f

and can be easily triggered with conformational transitions/structural changes under subtle changes of surroundings,[25–27] which are not possible by solution processing or complex multi-step manufacturing. Hence, developing ultrathin freestanding films using a simple way without additional processing or releasing steps is of great importance.

Silk is a natural biomaterial with many appealing properties including high biocompatibility, biodegradability, and mechanical strength,[28] which has been recognised as an excellent candidate for developing bio-integrated electronic devices.[29–32] Notably, silk possesses unique conformations that are critical in determining the performance and function of silk materials. For example, the random coil dominated uncrystallized structures are metastable and water soluble, while the β-sheet dominated crystallized structures are more thermodynamically stable. With proper conformation modulation, various programmed transient electronics,[33] biodegradable implants,[34] or responsive actuators[35] based on silk have been successfully developed. However, the uncrystallized secondary structures are easily triggered and changed by simple physical/chemical treatments like methanol soaking, mechanical drawing, and sonication,[36] making silk unsuitable for additional solution processing or transferring. Under these circumstances, it is highly desirable to develop freestanding ultrathin silk films while maintaining the uncrystallized structures by novel film preparation methods.

Blowing soap bubbles is a fun activity for children all around the world. When dipping the wand into the bubble solution, the solution stretches over the hole and forms a thin liquid film. With continuous blowing, the liquid film bends outward and forms a bubble.[37] The size, thickness and lifetime of the suspended liquid films or formed bubbles are tunable by varying the additives in the bubble solution.[38] When selecting proper materials, even freestanding dry films can be obtained after solvent evaporation.[39,40] The one-step film or bubble preparation process is quite simple, providing a great inspiration for simply and rapidly preparing freestanding sub-micron thick polymer films.

Qingsong Li

Dr Qingsong Li is an associate professor at the Shenzhen Institute of Advanced Technology, Chinese Academy of Sciences, China. He received his B. S. (2014) and Ph. D. (2019) degrees from Soochow University. During 2017–2018, he joined Prof. Chen Xiaodong's group as a visiting student at Nanyang Technological University, Singapore. His research mainly focuses on silk-based functional materials and stretchable epidermal electronics.

Inspired by bubble-blowing, here we developed a sub-micron thick freestanding silk film by dip-coating a closed-loop frame in concentrated silk aqueous solution (Fig. 1). The substrate-free silk films suspended on the frame are only hundreds of nanometres thick after drying, which can be tailored with different planar and non-planar geometric shapes *via* engineering the frames. The silk films have extremely smooth surfaces and show rainbow-like colours due to the thin film interference. Additionally, the naturally dried silk films possess random coil dominated uncrystallized structures, exhibiting high modulation ability and topographic adaptability. The semi-dried or vapor melted silk films can be conformally attached on fingertips without distorting the fingerprint ridges, showing high stability even under skin deformation and rubbing by fingers/textiles. By virtue of the conformational modulation through ethanol soaking, the sub-micron thick silk films were programmed as transient or durable electronics with controlled lifetimes from 0.3 s to 72 h. The merits of our method and the obtained sub-micron thick silk films have enabled various applications in thin film electronics including skin electrodes, transferred skin circuits and injectable electronics. This research opens a new avenue for preparing high-quality thin polymer films without the need for substrates and additional releasing steps, showing great promise for developing thin film electronics in wearable and biomedical applications.

Experimental section

Preparation of silk fibroin solution

The regenerated silk fibroin solution was prepared as previously reported.[41] Firstly, degummed *Bombyx mori* silk fibres were dissolved in 9.3 mol L^{-1} LiBr solution at 60 °C for 2 h. Subsequently, the obtained solution was dialyzed in deionized water using a cellulose dialysis membrane at room temperature for 3 days to remove LiBr. After that, the dialyzed silk solution was centrifuged at 8000 rpm for 20 min to remove impurities.

To get silk fibroin with high concentrations, the purified silk solution was concentrated through a reverse dialysis method.[42,43] In a typical process, 10 wt% polyethylene glycol (M_w = 10 000) aqueous solution was prepared at first. Then a proper amount of silk fibroin solution was filled into a dialysis membrane (MWCO 3.5 kDa, Spectra/Por, USA). After that, the filled dialysis membrane was placed into the polyethylene glycol solution for a certain time according to the desired fibroin concentration. Finally, the concentrated silk fibroin solution was collected and stored at 4 °C for use later.

Preparation of sub-micron thick freestanding silk films

The preparation of sub-micron thick freestanding silk films can be separated into several stages: firstly, a closed-loop frame made using polyethylene terephthalate or metal wire was completely immersed in silk fibroin solution (9.6 wt%) and held for 5 s. Then, the frame was taken out from the solu-

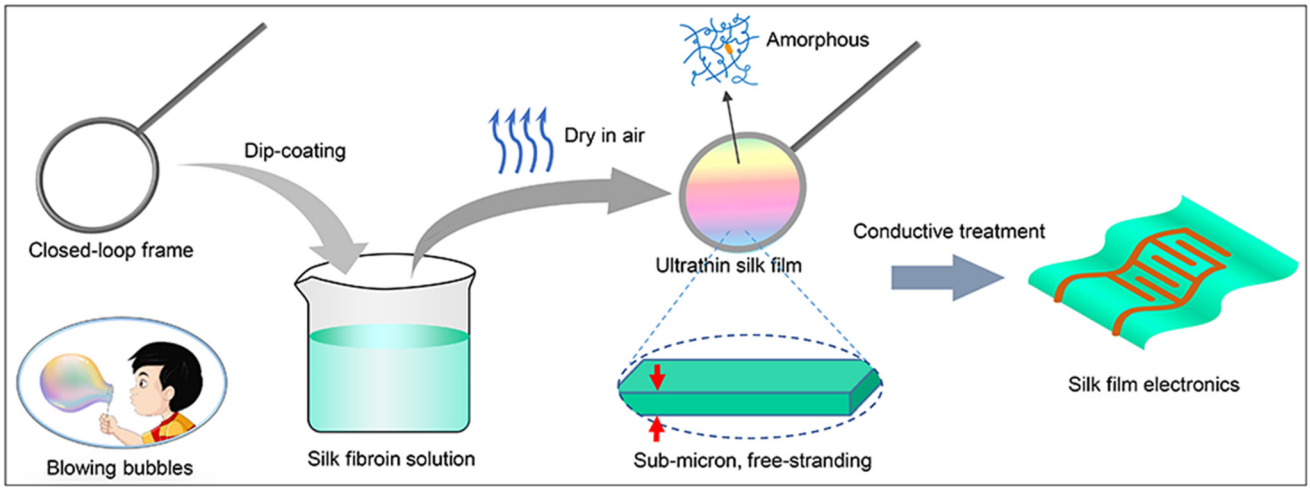

Fig. 1 Schematic illustration of the preparation process of sub-micron thick silk films on closed-loop frames and the corresponding silk film electronics.

tion carefully and a liquid film could be seen on the frame. Excess liquid was removed by filter paper from the lower edge of the frame. During solvent evaporation, the liquid film gradually changed from colourless to iridescent. Note that vibration and air flow are avoided during the film formation process. After drying for about 15–20 min, a rainbow-like thin silk film was obtained. To get silk films with different thicknesses, silk fibroin solutions with concentrations of 9.6, 13.3, 16.4, 19.8 wt% were used. When using highly concentrated silk fibroin solutions, no iridescence was observed during the film preparation due to the increased film thickness. The ambient temperature and humidity were 20–23 °C and 40–50% during preparation of the silk films.

Fabrication of transient and durable silk film circuits

The transient silk circuits were prepared by sputtering a thin layer of gold film on the as-prepared uncrystallized silk film by a direct-current magnetron sputtering system (sputtering power: 150 W; argon flow rate: 65 sccm; pressure: 3.8 Pa; sputtering time: 10 s) *via* a shadow mask.[44] A micro-LED was connected using silver paste to indicate the working conditions of the circuits. To prepare the durable silk circuits, the silk films were firstly pre-treated using 75% ethanol to increase the crystallinity and make the silk film insoluble. Then, poly(3,4-ethylenedioxythiophene):polystyrene sulfonate (PEDOT:PSS) aqueous solution (Clevios PH 1000) with 5 vol% glycerol and 0.5 vol% Triton X-100 were painted on the silk film with desired circuit patterns. After natural drying, the films were thermally annealed at 120 °C for 15 min to stabilize the PEDOT:PSS and improve its conductivity.

Preparation of silk film electrodes and EMG signal recording

Ethanol-treated silk films were dip-coated in PEDOT:PSS solution which contained 5 vol% glycerol and 0.5 vol% Triton X-100, followed by air-drying and thermal annealing to obtain the silk film electrodes. The obtained electrodes were placed on the skin surface of flexor carpi ulnaris to record the muscle activities during making fists. Before EMG measurement, the interfacial impedance was tested under the calm state using an electrochemical workstation (CHI760E, CH Instruments, Inc.). The hand grip at different force levels was recorded by a home-customized toolkit (sampling frequency = 2 kHz, SNR > 100 dB, common mode rejection ratio > 90 dB). The commonly used commercial electrodes which are mainly composed of a Ag/AgCl plate surrounded by a conductive gel (Cathay Manufacturing Corp., China) were chosen as comparison, as shown in Fig. S1.†

Characterization

The surface morphology of freestanding silk films and their thickness were characterized using an atomic force microscope (AFM) system (Bruker Nano Inc., USA) in tapping mode and a field emission microscope (S-4800, Hitachi Ltd, Japan). When measuring the thickness, the sampling points should be kept away from the edge of the frame at least 4 mm. A Thermo Nicolet 5700 FTIR spectrometer (Thermo Fisher Scientific Inc., USA) was used to analyse the silk fibroin conformation. The transmission spectrum of silk film was collected by a fibre-optic spectrometer (PG2000-Pro, Ideaoptics Instruments) with a wavelength range of 300–1100 nm. The mechanical properties of the ultrathin untreated and ethanol-treated silk films (prepared using 9.6 wt% silk solution) were measured using a mechanical tester (AG-X Plus 100N, Shimadzu, Japan) with a controlled sample size of 1 × 1 cm and a constant tension speed of 10 mm min^{-1}. The resistance change under strain of the silk film electrode was measured with a semiconductor parameter analyser (Keithley 2000 multimeter, Tektronix) while strain was applied by the mechanical tester at a speed of 10 mm min^{-1}. Before tension, the sample was pasted on a polyurethane tape and the sample size was maintained at 1 cm (length) × 0.5 cm (width).

Results and discussion

The typical process inspired by bubble-blowing for fabricating the freestanding sub-micron thick silk film is shown in Fig. 1. The used regenerated silk fibroin solution was obtained from cocoons of the *Bombyx mori* silkworm after several processing procedures including degumming, dissolution, dialysis, and concentration. When a closed-loop frame was completely immersed in the silk solution and taken out vertically, a liquid film was suspended on the frame. Due to the influence of gravity, the liquid film become very thin with a gradient thickness from the top to the bottom of the frame. Notably, silk fibroin exhibits an amphiphilic characteristic due to the highly repetitive amino acid sequences with alternating hydrophobic and hydrophilic blocks along the molecular chains, thus being capable of absorbing at the air–water interface.[45] The hydrophobic regions of the fibroin chains lead to an affinity to the air phase and enable silk fibroin to form stable viscoelastic films at the air–water interface, which in turn can stabilize the liquid film.[46] Normally, the evaporation of water in a liquid film decreases the film thickness and leads to the rupture of film. Considerable intermolecular interactions in the highly concentrated silk solution are favourable for film formation and stabilization. After water had evaporated fully, the thin liquid film became dried, and an iridescent substrate-free silk film was obtained (Fig. 2a). The film consists of entangled fibroin chains, showing high robustness and self-supporting characteristics after removing the frame (Fig. 2b), which provides possibilities for further processing or use. The as-prepared thin silk film is highly transparent with optical transmission more than 80% across the visible spectrum (Fig. 2c), and the printed picture can be clearly seen through the film (Fig. 2c, inset). Interestingly, there are some ripples in the transmission spectrum which result from the interference of light reflected from the top and bottom surfaces of the films, indicating the film thickness is comparable to the wavelength of visible light. The cross-sectional view and profile of the iridescent silk film on a silicon wafer prepared by semi-dried liquid film show that their thicknesses are only hundreds of nanometres (Fig. S2†) after drying, which further verifies the speculation. Like soap bubbles, the thickness of the dried silk film is highly related to numerous factors including solution concentration, frame placement, and ambient conditions. By using silk fibroin solutions with different concentrations, freestanding silk films with different thicknesses ranging from hundreds of nanometres to several micrometres are readily obtained (Fig. S3†), showing high controllability. Although a lower concentration of silk fibroin solution trends to form thinner silk films, very low concentration of the solution, *i.e.*, 5–8 wt% or lower, will make the liquid film rupture easily before drying. A typical thin film with a thickness of only ~150 nm is shown in Fig. 2d. Further optimization can be conducted to more precisely control the film thickness and size for other purposes. The silk film has an extremely flat surface, no impurities are observed even in the microscale level (Fig. 2e), which is favourable for displaying bright colours. The

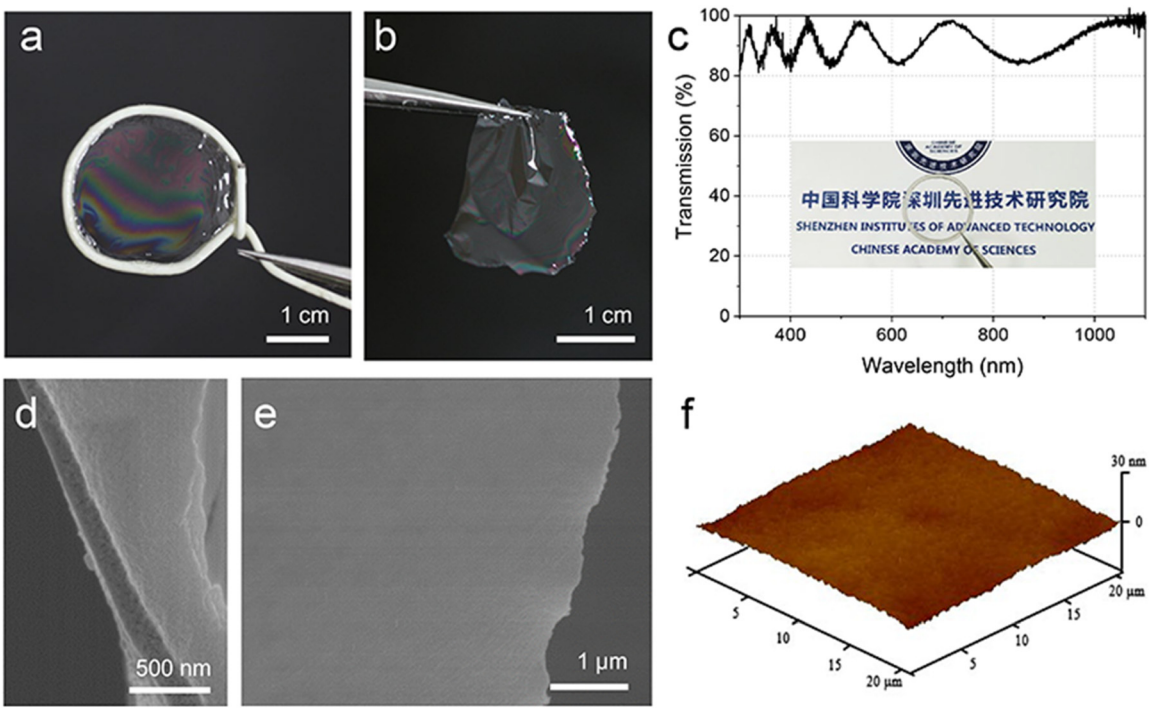

Fig. 2 The pictures and morphologies of the prepared sub-micron thick silk films. (a) Optical image of the sub-micron thick silk film with iridescent colours on a closed-loop frame. (b) The silk film taken off from the frame. (c) Transmission spectrum of the sub-micron thick silk film; inset: photograph of the silk film covered on a printed picture showing the high transparency. (d) Sectional view of the silk film. (e) SEM image of the silk film showing high smoothness. (f) AFM image showing the surface morphologies of the silk film.

surface topography of the silk film was characterized by AFM in tapping mode, as shown in Fig. 2f. Within a length scale of 20 μm, the root mean square roughness (R_q) is less than 3 nm, which is comparable to that of many other silk films prepared by the spin-coating process.[47] Considering the low thickness and roughness, the sub-micron thick silk films are ideal substates for microelectronic sensors or optoelectronic devices.

When a closed-loop is dipped into a silk fibroin solution, the surface of the liquid film that forms represents the minimum mathematically possible area for the loop.[48] Therefore, using specific closed-loop frames allows the formation of freestanding films with different geometric shapes like circles, squares, triangles, and even non-planar topologies (Fig. 3a–d). Similarly, spherical shape can be obtained when the silk solution bubble is formed due to the minimized surface energy for a given volume. Once the bubble has reached the wetted substrate, it adopts a static shape that is governed by the balance between the surface tension and buoyancy effects.[49] During water evaporation and film drying, the highly concentrated silk fibroin solution can solidify to form a polymer film. When the size of the spherical silk bubble is small, the strength of the dried silk can maintain the spherical shape of the silk film, and no collapse is observed (Fig. 3e). This strategy enables the preparation of silk films with desirable topologies and unique geometries, which cannot be realized using other methods. The naturally dried silk is amorphous with random coil dominated structures, giving the sub-micron thick silk films high modulation ability and plasticity. Typically, the silk films with thickness of about hundreds of nanometres exhibit more interesting and unique properties when compared with thick films. For example, uncrystallized silk has a strong affinity to water, endowing the sub-micron thick silk film with high humidity sensitivity with an obvious volume expansion when exposed to water vapor (Video 1†). Furthermore, the semi-dried or water vapor melted silk film shows low bending stiffness and high shape adaptability, which can be conformally attached on curved skin like fingertips (Fig. 3f) while keeping the fingerprints visible (Fig. 3g). The optical image in Fig. 3h shows that the thin silk film can adhere to soft skin with a snug fit over the micrometre-scale topologies and give the film high stability even during mechanical compression (Fig. 3i). Furthermore, no detachment or delamination of the silk film on skin is observed after rubbing by fingers and textiles (Video 2†), indicating high robustness during on-skin use. In addition, the sub-micron thick silk films are lightweight, which can be wrapped and rolled on human hair (Fig. 3j and k). The conformal capability and lightweight characteristics of the thin silk films show potential for seamless integration of wearable skin electronics with curved and dynamic biological substrates.

Silk fibroin possesses unique protein conformations that are capable of being tuned by proper chemical and physical treatments, giving the silk films diverse properties and performance. For the regenerated silk with uncrystallized structures, the random coils and/or helixes are metastable, making the films soluble in water. However, when the uncrystallized silk films are treated by ethanol soaking, the random coil and/or helix dominated silk conformation will convert to stable β-sheet structures. The stabilization process endows the sub-micron thick silk films with high structure stability, which can tolerate soaking in various solvents (Fig. 4a). The structure modification and conformation transition of silk was monitored by Fourier transform infrared spectroscopy (FTIR). As shown in Fig. 4b, the characteristic amide I absorption band in the FTIR spectra shifts from 1636 cm^{-1} to 1618 cm^{-1} after ethanol treatment, representing an increased content of

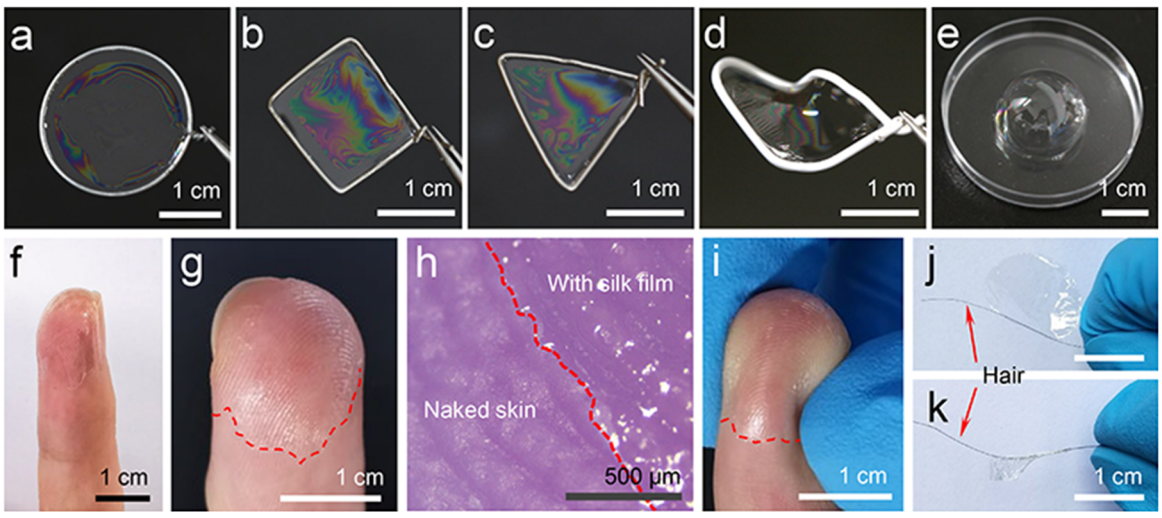

Fig. 3 The controlled geometric shapes and conformality of sub-micron thick silk films. The silk films on the frames with various shapes like (a) circles, (b) squares, (c) triangles, and (d and e) even non-planar topologies. (f) The sub-micron thick silk film on curved fingertip with (g) clear fingerprints and (i) high mechanical stability. (h) Optical microscope image of the sub-micron thick silk film on fingertip. Photographs of the silk films (j) wrapped and (k) rolled on human hair.

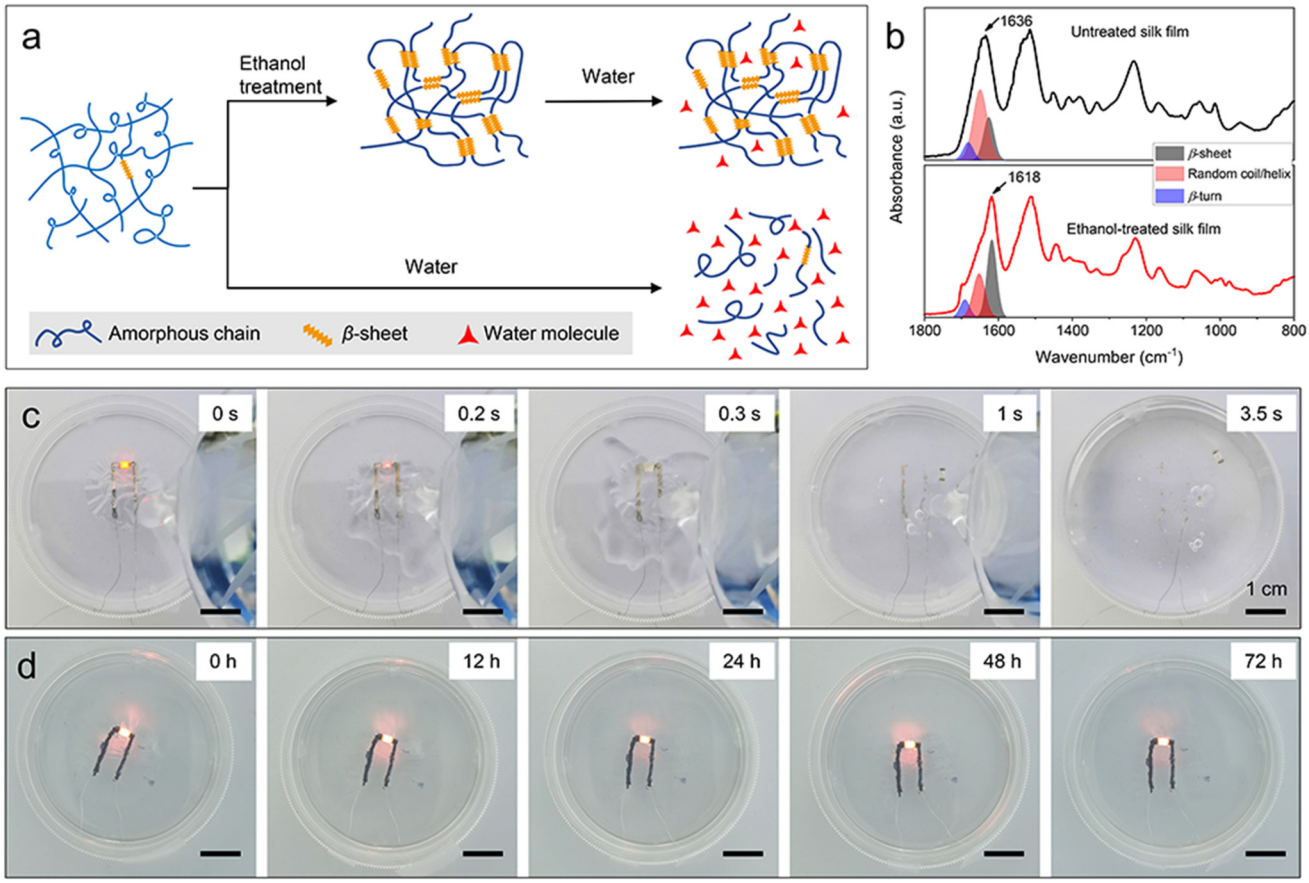

Fig. 4 Modulation of silk films for transient and durable electronics. (a) A schematic illustration showing the mechanism of water stability for the untreated and ethanol-treated silk films. (b) FTIR spectra of untreated and ethanol-treated silk films. (c) Sequential photographs of water induced deconstruction of silk film circuits based on untreated silk film and gold layer. (d) Photographs of the durable silk film circuits based on ethanol-treated silk films and PEDOT:PSS in water for 72 h.

β-sheet. To further quantify the variation of β-sheet content, deconvolution of the FTIR spectrum in the broadband from 1580 to 1720 cm^{-1} was performed.[50] The contents of β-sheet in the regenerated silk and ethanol-treated silk are calculated to be 22.8%, and 47.3%, respectively, indicating that simple ethanol treatment can effectively tune the crystalline structure of silk and give it high stability. Besides, the ethanol treatment also significantly modified the mechanical strength of the thin silk films. Both the untreated and ethanol-treated ultrathin silk films exhibit good mechanical properties, ensuring the self-supporting ability and stability during use (Fig. S4†). After ethanol soaking, the silk films show higher stiffness due to the increased β-sheet structures.

Based on these characteristics, the sub-micron thick silk films are suitable to be engineered as transient or durable electronics when being deposited with conducting patterns. Fig. 4c provides a set of images showing the transient behaviours of the electronic circuits based on uncrystallized silk film and thin gold film in response to DI water at room temperature. The uncrystallized fibroin films rapidly dissolve in water with the deconstruction of the nano gold layer above, and the operated light-emitting diode (LED) fails to work within 0.3 s in gently flowing water or 0.5 s when being totally immersed in water without flowing. It is observed that the electronic circuits completely disappear in water after only several seconds (Video 3†), demonstrating fast transience, which is much faster than many other reported transient electronics.[25,51,52] However, when the sub-micron thick silk film is pre-treated with ethanol, the electronic circuit can maintain the structure integrity and working stability for more than 72 h in water, showing high durability for long-term use (Fig. 4d). These results indicate that the sub-micron thick silk film based electronic devices are highly programmable, which are potentially suitable for developing disposable devices or electronics with controllable lifetime and diverse properties using one material.

By combining the shape adaptability of the semi-dried uncrystallized silk film and the substrate-free film preparation process, microelectronics can be easily transferred and conformally adhered on skin, as shown in Fig. 5a. When a closed-loop frame was dip-coated in the fibroin solution, the floating circuit was simultaneously taken out and supported by the liquid film. After semi-drying, the silk film with circuit could be attached on a finger simply. Owing to the low thickness of

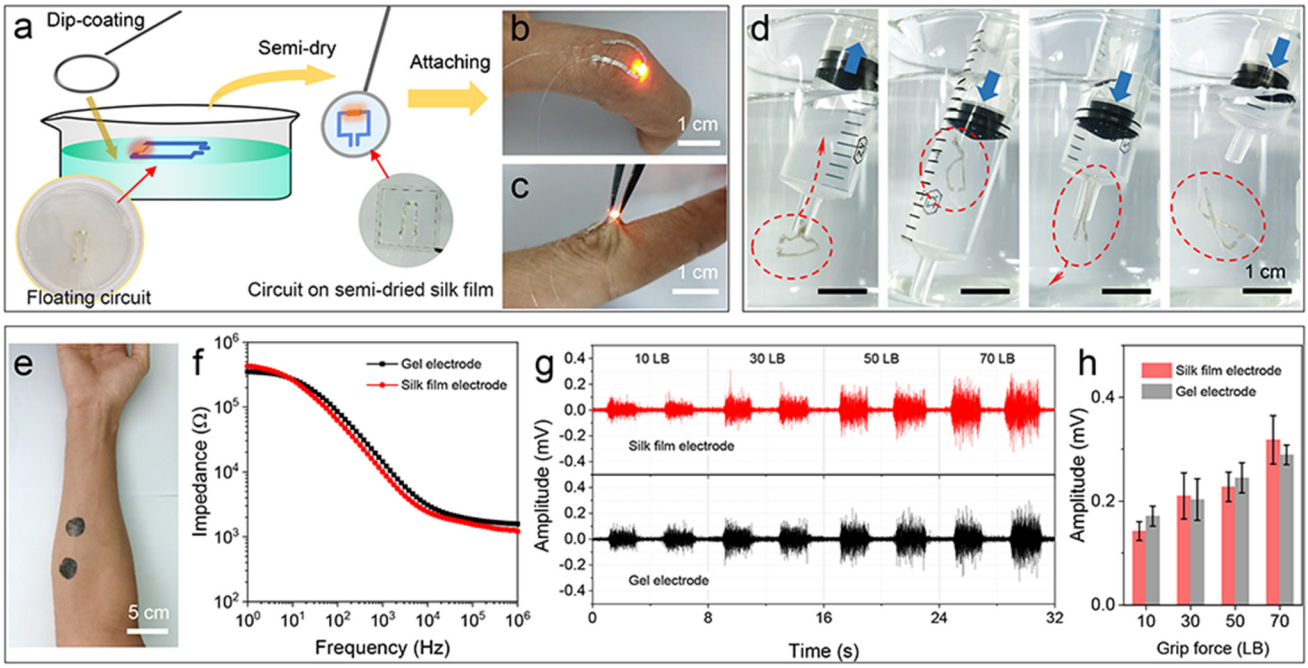

Fig. 5 Potential applications of silk film electronics for (a–c) transferring printed circuits, (d) injectable electronics, and (e–h) skin electrodes. (a) Schematic diagram of the transfer procedures of thin electronic circuits using dip-coating technique and semi-dried silk film. (b) The transferred circuits on wrinkled skin. (c) The adhesion stability of transferred circuits on skin. (d) Images of thin silk film electronics injected through a tube into PBS solution. (e) The photograph of silk film electrodes on the arm using PEDOT:PSS coated ethanol-treated silk film. (f) The skin interface impedance of silk film electrodes and commercial gel electrodes. (g) EMG signals recorded by the silk film electrodes and commercial gel electrodes when making fists with different gripping forces. (h) Amplitudes of the EMG signals recorded by the two electrodes.

the silk film, the circuit conforms well with the wrinkles and no disturbance of the circuit deformation is observed (Fig. 5b). Furthermore, silk fibroin has been reported to have adhesive properties to various substates like biological tissues,[53,54] thus the semi-dried silk film also acts as a binder layer and gives the electronic circuit high stability on skin, which can withstand cyclic skin deformation and mechanical stretching (Fig. 5c).

Benefiting from the high stability of the ethanol-treated sub-micron thick silk film in water, it can be potentially used as foldable and injectable bioelectronics without designing complex structures when combing with the feature of low thickness. It is notable that water molecules can significantly decrease the modulus of silk down to kilopascals;[55,56] thus, the sub-micron thick silk film shows low bending stiffness in aqueous environments. When a 1 × 2 cm silk film circuit that based on crystallized sub-micron thick silk film and nano gold is immersed in phosphate buffered saline (PBS) solution, it can be freely loaded into a syringe and injected through the tube with an inner diameter of 2 mm (Fig. 5d), which is similar to the reported injectable mesh electronics.[57] During this process, the silk film circuit maintains high structural integrity after compressing and unfolding multiple times (Video 4†). These results demonstrate the possibilities of delivering flexible electronics into internal cavities, showing great promise for developing noninvasive implanted bioelectronics.

As a natural protein, silk fibroin is biocompatible and has been widely used in biosignal measurement for potential clinical diagnosis and motion monitoring. By virtue of the low thickness and stiffness, the sub-micron thick silk film is suitable to be used as conformal skin electrodes for recording electrophysiological signals when incorporating with conducting polymer PEDOT:PSS by surface coating.[56] The silk film electrodes show high stretchability up to > 120% (Fig. S5†) due to the plasticization of doped glycerol in aqueous PEDOT:PSS,[58] ensuring the mechanical reliability when being used on stretchable and moving skin. The silk film electrodes are highly conformal on skin (Fig. 5e), exhibiting as low interfacial impedance with skin as the commercial gel electrodes (Fig. 5f), which is crucial for the signal integrity during use. As shown in Fig. 5g, the electromyography (EMG) signals generated from the muscle activities were detected *via* applying 10, 30, 50, and 70 LB of gripping force to the gripper, and a steady increase in signal intensity can be observed with the increase of the gripping forces. Furthermore, the EMG signals collected by the silk electrodes show comparable amplitude to the commercial gel electrodes under the same gripping force (Fig. 5h). Besides, the silk film electrodes lead to no remarkable skin irritation after wearing for 12 h, while commercial gel electrodes cause skin discomfort and over-soaking (Fig. S6†), which means the silk film electrodes are suitable for long-term use.

Conclusions

In summary, we demonstrate a facile method for the fabrication of sub-micron thick freestanding silk films inspired by bubble-blowing. By dip-coating a closed-loop frame in concentrated silk fibroin aqueous solution, substrate-free silk films with bright rainbow-like colours can be easily produced after drying. These films show high surface smoothness and have thickness down to hundreds of nanometres, which can be conformally attached on curved fingertips without distorting the fingerprint structures. The conformations determine the diverse properties of silk, giving the naturally dried silk film high modulation ability, which can be programmed as transient circuits with water-triggered rapid decomposition or durable electronic circuits for long-term use. The simple film preparation method, combined with the intrinsic adhesion of uncrystallized silk, was successfully utilized to transfer printed microelectronics to skin and give it high adhesion. Furthermore, the ethanol-treated silk films exhibit high structural stability which can tolerate solution processing, enabling applications for wearable skin electrodes and injectable ultrathin electronic circuits. In particular, the silk film electrodes are able to record EMG signals with high quality comparable to commercial gel electrodes, and do not lead to discomfort during long-term use. These results prove that our method and obtained sub-micron thick silk films possess superior advantages to many other strategies and thin films, showing great promise for developing versatile films and related electronic devices.

Author contributions

Qingsong Li: conceptualization, methodology, formal analysis, investigation, fund acquisition, writing – original draft, writing – review and editing, and project administration. Jing Sun: investigation. Fengjiao Bai: investigation. Xiaomeng Zhou: methodology. Wei Yuan: methodology. Jin Lin: investigation. Ke-Qin Zhang: conceptualization. Guanglin Li: resources and fund acquisition. Zhiyuan Liu: fund acquisition and resources.

Conflicts of interest

There are no conflicts to declare.

Acknowledgements

This work was supported by the National Natural Science Foundation of China (62201559 and U81927804), the NSFC-Shenzhen Robotics Basic Research Center Program (U2013207), the Guangdong Basic and Applied Basic Research Foundation (2021A1515110879), and National Key R&D Program of China (2021YFF0501600).

References

1 I. Kim, K. Woo, Z. Zhong, P. Ko, Y. Jang, M. Jung, J. Jo, S. Kwon, S. H. Lee, S. Lee, H. Youn and J. Moon, *Nanoscale*, 2018, **10**, 7890–7897.
2 C. Liang, Y. Liu, W. Lu, G. Tian, Q. Zhao, D. Yang, J. Sun and D. Qi, *Nanoscale*, 2022, **14**, 3346–3366.
3 A. Abramson, C. T. Chan, Y. Khan, A. Mermin-Bunnell, N. Matsuhisa, R. Fong, R. Shad, W. Hiesinger, P. Mallick, S. S. Gambhir and Z. Bao, *Sci. Adv.*, 2022, **8**, eabn6550.
4 T. Someya, Z. Bao and G. G. Malliaras, *Nature*, 2016, **540**, 379–385.
5 J. W. Jeong, W. H. Yeo, A. Akhtar, J. J. Norton, Y. J. Kwack, S. Li, S. Y. Jung, Y. Su, W. Lee, J. Xia, H. Cheng, Y. Huang, W. S. Choi, T. Bretl and J. A. Rogers, *Adv. Mater.*, 2013, **25**, 6839–6846.
6 D. H. Kim, J. Viventi, J. J. Amsden, J. Xiao, L. Vigeland, Y. S. Kim, J. A. Blanco, B. Panilaitis, E. S. Frechette, D. Contreras, D. L. Kaplan, F. G. Omenetto, Y. Huang, K. C. Hwang, M. R. Zakin, B. Litt and J. A. Rogers, *Nat. Mater.*, 2010, **9**, 511–517.
7 S. Y. Liu, Y. F. Rao, H. Jang, P. Tan and N. S. Lu, *Matter*, 2022, **5**, 1104–1136.
8 Z. Yan, D. Xu, Z. Lin, P. Wang, B. Cao, H. Ren, F. Song, C. Wan, L. Wang, J. Zhou, X. Zhao, J. Chen, Y. Huang and X. Duan, *Science*, 2022, **375**, 852–859.
9 M. Kaltenbrunner, T. Sekitani, J. Reeder, T. Yokota, K. Kuribara, T. Tokuhara, M. Drack, R. Schwodiauer, I. Graz, S. Bauer-Gogonea, S. Bauer and T. Someya, *Nature*, 2013, **499**, 458–463.
10 K. Fukuda, Y. Takeda, Y. Yoshimura, R. Shiwaku, L. T. Tran, T. Sekine, M. Mizukami, D. Kumaki and S. Tokito, *Nat. Commun.*, 2014, **5**, 4147.
11 G. A. Salvatore, N. Munzenrieder, T. Kinkeldei, L. Petti, C. Zysset, I. Strebel, L. Buthe and G. Troster, *Nat. Commun.*, 2014, **5**, 2982.
12 R. A. Nawrocki, H. Jin, S. Lee, T. Yokota, M. Sekino and T. Someya, *Adv. Funct. Mater.*, 2018, **28**, 1803279.
13 L. M. Ferrari, S. Sudha, S. Tarantino, R. Esposti, F. Bolzoni, P. Cavallari, C. Cipriani, V. Mattoli and F. Greco, *Adv. Sci.*, 2018, **5**, 1700771.
14 J. J. Richardson, M. Bjornmalm and F. Caruso, *Science*, 2015, **348**, aaa2491.
15 Y. Zhao, S. Zhang, T. Yu, Y. Zhang, G. Ye, H. Cui, C. He, W. Jiang, Y. Zhai, C. Lu, X. Gu and N. Liu, *Nat. Commun.*, 2021, **12**, 4880.
16 M. Takakuwa, K. Fukuda, T. Yokota, D. Inoue, D. Hashizume, S. Umezu and T. Someya, *Sci. Adv.*, 2021, **7**, eabl6228.
17 S. Tang, J. Gong, Y. Shi, S. Wen and Q. Zhao, *Nat. Commun.*, 2022, **13**, 3227.
18 Y. Wang, T. Hong, L. Wang, G. Li, N. Bai, C. Li, P. Lu, M. Cai, Z. Wu, N. Lu, B. Yu, J. Zhang and C. F. Guo, *Mater. Today Phys.*, 2020, **12**, 100191.
19 Y. J. Fan, X. Li, S. Y. Kuang, L. Zhang, Y. H. Chen, L. Liu, K. Zhang, S. W. Ma, F. Liang, T. Wu, Z. L. Wang and G. Zhu, *ACS Nano*, 2018, **12**, 9326–9332.

20 A. Miyamoto, S. Lee, N. F. Cooray, S. Lee, M. Mori, N. Matsuhisa, H. Jin, L. Yoda, T. Yokota, A. Itoh, M. Sekino, H. Kawasaki, T. Ebihara, M. Amagai and T. Someya, *Nat. Nanotechnol.*, 2017, **12**, 907–913.
21 Y. Wang, S. Lee, H. Wang, Z. Jiang, Y. Jimbo, C. Wang, B. Wang, J. J. Kim, M. Koizumi, T. Yokota and T. Someya, *Proc. Natl. Acad. Sci. U. S. A.*, 2021, **118**, e2111904118.
22 D. Gao, J. Lv and P. S. Lee, *Adv. Mater.*, 2022, **34**, 2105020.
23 W. B. Han, J. H. Lee, J. W. Shin and S. W. Hwang, *Adv. Mater.*, 2020, **32**, 2002211.
24 T. Lei, M. Guan, J. Liu, H. C. Lin, R. Pfattner, L. Shaw, A. F. McGuire, T. C. Huang, L. Shao, K. T. Cheng, J. B. Tok and Z. Bao, *Proc. Natl. Acad. Sci. U. S. A.*, 2017, **114**, 5107–5112.
25 Y. Gao, Y. Zhang, X. Wang, K. Sim, J. Liu, J. Chen, X. Feng, H. Xu and C. Yu, *Sci. Adv.*, 2017, **3**, e1701222.
26 L. Yin, H. Y. Cheng, S. M. Mao, R. Haasch, Y. H. Liu, X. Xie, S. W. Hwang, H. Jain, S. K. Kang, Y. W. Su, R. Li, Y. G. Huang and J. A. Rogers, *Adv. Funct. Mater.*, 2014, **24**, 645–658.
27 J. Magoshi, Y. Magoshi, M. A. Becker, M. Kato, Z. Han, T. Tanaka, S. Inoue and S. Nakamura, *Thermochim. Acta*, 2000, **352**, 165–169.
28 L. D. Koh, Y. Cheng, C. P. Teng, Y. W. Khin, X. J. Loh, S. Y. Tee, M. Low, E. Y. Ye, H. D. Yu, Y. W. Zhang and M. Y. Han, *Prog. Polym. Sci.*, 2015, **46**, 86–110.
29 B. Zhu, H. Wang, W. R. Leow, Y. Cai, X. J. Loh, M. Y. Han and X. Chen, *Adv. Mater.*, 2016, **28**, 4250–4265.
30 C. Wang, K. Xia, Y. Zhang and D. L. Kaplan, *Acc. Chem. Res.*, 2019, **52**, 2916–2927.
31 C. Shi, F. Hu, R. Wu, Z. Xu, G. Shao, R. Yu and X. Y. Liu, *Adv. Mater.*, 2021, **33**, 2005910.
32 L. Cao, Q. Liu, J. Ren, W. Chen, Y. Pei, D. L. Kaplan and S. Ling, *Adv. Mater.*, 2021, **33**, 2102500.
33 S. W. Hwang, H. Tao, D. H. Kim, H. Cheng, J. K. Song, E. Rill, M. A. Brenckle, B. Panilaitis, S. M. Won, Y. S. Kim, Y. M. Song, K. J. Yu, A. Ameen, R. Li, Y. Su, M. Yang, D. L. Kaplan, M. R. Zakin, M. J. Slepian, Y. Huang, F. G. Omenetto and J. A. Rogers, *Science*, 2012, **337**, 1640–1644.
34 H. Tao, S. W. Hwang, B. Marelli, B. An, J. E. Moreau, M. Yang, M. A. Brenckle, S. Kim, D. L. Kaplan, J. A. Rogers and F. G. Omenetto, *Proc. Natl. Acad. Sci. U. S. A.*, 2014, **111**, 17385–17389.
35 Z. Yin, S. L. Shi, X. P. Liang, M. C. Zhang, Q. S. Zheng and Y. Y. Zhang, *Adv. Fiber Mater.*, 2019, **1**, 197–204.
36 C. Li, J. Wu, H. Shi, Z. Xia, J. K. Sahoo, J. Yeo and D. L. Kaplan, *Adv. Mater.*, 2022, **34**, 2105196.
37 How to Blow Bubbles, **https://www.wikihow.com/Blow-Bubbles**, (accessed September, 2022).
38 S. Frazier, X. Y. Jiang and J. C. Burton, *Phys. Rev. Fluids*, 2020, **5**, 013304.
39 W. Chen and L. Yan, *Adv. Mater.*, 2012, **24**, 6229–6233.
40 X. Q. Yang, L. H. Li, S. Q. Wang, Q. F. Lu, Y. Y. Bai, F. Q. Sun, T. Li, Y. Li, Z. H. Wang, Y. Y. Zhao, Y. X. Shi and T. Zhang, *Adv. Electron. Mater.*, 2020, **6**, 2000306.
41 Q. S. Li, N. Qi, Y. Peng, Y. F. Zhang, L. Shi, X. H. Zhang, Y. K. Lai, K. Wei, I. S. Kim and K. Q. Zhang, *RSC Adv.*, 2017, **7**, 17889–17897.
42 J. S. Liao, K. A. Pham and V. Breedveld, *ACS Sustainable Chem. Eng.*, 2021, **9**, 9671–9679.
43 D. N. Rockwood, R. C. Preda, T. Yucel, X. Q. Wang, M. L. Lovett and D. L. Kaplan, *Nat. Protoc.*, 2011, **6**, 1612–1631.
44 Q. S. Li, C. Ding, W. Yuan, R. J. Xie, X. M. Zhou, Y. Zhao, M. Yu, Z. J. Yang, J. Sun, Q. Tian, F. Han, H. F. Li, X. P. Deng, G. L. Li and Z. Y. Liu, *Adv. Fiber Mater.*, 2021, **3**, 302–311.
45 Y. H. Yang, C. Dicko, C. D. Bain, Z. G. Gong, R. M. J. Jacobs, Z. Z. Shao, A. E. Terry and F. Vollrath, *Soft Matter*, 2012, **8**, 9705–9712.
46 X. Y. Qiao, R. Miller, E. Schneck and K. Sun, *Soft Matter*, 2020, **16**, 3695–3704.
47 A. Bucciarelli, V. Mulloni, D. Maniglio, R. K. Pal, V. K. Yadavalli, A. Motta and A. Quaranta, *Opt. Mater.*, 2018, **78**, 407–414.
48 M. Ueno, N. Isokawa, K. Fueda, S. Nakahara, H. Teshima, N. Yamamoto, H. Yokoyama, Y. Noritsugu, K. Shibata, K. Miyagawa, S. Tanaka, T. Hirano, A. Fujito, A. Takashima and K. Kanno, *World J. Chem. Educ.*, 2016, **4**, 32–44.
49 J. Miguet, F. Rouyer and E. Rio, *Molecules*, 2021, **26**, 1317.
50 C. Guo, J. Zhang, J. S. Jordan, X. Wang, R. W. Henning and J. L. Yarger, *Biomacromolecules*, 2018, **19**, 906–917.
51 L. Teng, S. C. Ye, S. Handschuh-Wang, X. H. Zhou, T. S. Gan and X. C. Zhou, *Adv. Funct. Mater.*, 2019, **29**, 1808739.
52 H. Wang, B. Zhu, X. Ma, Y. Hao and X. Chen, *Small*, 2016, **12**, 2715–2719.
53 E. R. Johnston, Y. Miyagi, J. A. Chuah, K. Numata and M. A. Serban, *ACS Biomater. Sci. Eng.*, 2018, **4**, 2815–2824.
54 C. J. Love, B. A. Serban, T. Katashima, K. Numata and M. A. Serban, *ACS Biomater. Sci. Eng.*, 2019, **5**, 5960–5967.
55 B. D. Lawrence, S. Wharram, J. A. Kluge, G. G. Leisk, F. G. Omenetto, M. I. Rosenblatt and D. L. Kaplan, *Macromol. Biosci.*, 2010, **10**, 393–403.
56 Q. Li, G. Chen, Y. Cui, S. Ji, Z. Liu, C. Wan, Y. Liu, Y. Lu, C. Wang, N. Zhang, Y. Cheng, K. Q. Zhang and X. Chen, *ACS Nano*, 2021, **15**, 9955–9966.
57 J. Liu, T. M. Fu, Z. Cheng, G. Hong, T. Zhou, L. Jin, M. Duvvuri, Z. Jiang, P. Kruskal, C. Xie, Z. Suo, Y. Fang and C. M. Lieber, *Nat. Nanotechnol.*, 2015, **10**, 629–636.
58 S. Lu, X. Wang, Q. Lu, X. Zhang, J. A. Kluge, N. Uppal, F. Omenetto and D. L. Kaplan, *Biomacromolecules*, 2010, **11**, 143–150.